THE JOURNAL OF BIOLOGICAL CHEMISTRY VOL. 287, NO. 23, pp. 19631–19641, June 1, 2012
© 2012 by The American Society for Biochemistry and Molecular Biology, Inc. Published in the U.S.A.

S-Palmitoylation and Ubiquitination Differentially Regulate Interferon-induced Transmembrane Protein 3 (IFITM3)-mediated Resistance to Influenza Virus*[S]

Received for publication, March 14, 2012, and in revised form, April 11, 2012 Published, JBC Papers in Press, April 17, 2012, DOI 10.1074/jbc.M112.362095

Jacob S. Yount, Roos A. Karssemeijer, and Howard C. Hang[1]

From the Laboratory of Chemical Biology and Microbial Pathogenesis, The Rockefeller University, New York, New York 10065

Background: IFITM3 is a protein of the innate immune system that inhibits viral infections.
Results: *S*-palmitoylation enhances IFITM3 membrane affinity and antiviral activity, whereas ubiquitination decreases endolysosome localization and antiviral activity.
Conclusion: IFITM3 is dually and opposingly regulated by posttranslational modifications, and study of these modifications has led to an unpredicted intramembrane topology model.
Significance: Understanding modes of IFITM3 regulation is critical for dissecting molecular mechanisms controlling viral inhibition.

The interferon (IFN)-induced transmembrane protein 3 (IFITM3) is a cellular restriction factor that inhibits infection by influenza virus and many other pathogenic viruses. IFITM3 prevents endocytosed virus particles from accessing the host cytoplasm although little is known regarding its regulatory mechanisms. Here we demonstrate that IFITM3 localization to and antiviral remodeling of endolysosomes is differentially regulated by *S*-palmitoylation and lysine ubiquitination. Although *S*-palmitoylation enhances IFITM3 membrane affinity and antiviral activity, ubiquitination decreases localization with endolysosomes and decreases antiviral activity. Interestingly, autophagy reportedly induced by IFITM3 expression is also negatively regulated by ubiquitination. However, the canonical ATG5-dependent autophagy pathway is not required for IFITM3 activity, indicating that virus trafficking from endolysosomes to autophagosomes is not a prerequisite for influenza virus restriction. Our characterization of IFITM3 ubiquitination sites also challenges the dual-pass membrane topology predicted for this protein family. We thus evaluated topology by *N*-linked glycosylation site insertion and protein lipidation mapping in conjunction with cellular fractionation and fluorescence imaging. Based on these studies, we propose that IFITM3 is predominantly an intramembrane protein where both the N and C termini face the cytoplasm. In sum, by characterizing *S*-palmitoylation and ubiquitination of IFITM3, we have gained a better understanding of the trafficking, activity, and intramembrane topology of this important IFN-induced effector protein.

Type I interferons (IFNs) are cytokines that activate host pathways to inhibit the replication of viruses (1). Highlighting the importance of this innate system of defense, humans deficient in components of type I IFN signaling are particularly vulnerable to viral disease (2). IFNs limit viral infections through the induction of hundreds of IFN-stimulated genes, but the antiviral mechanism(s) for many of these genes remains to be determined (3–7). The IFN-induced transmembrane (IFITM)[2] protein family was recently shown to mediate a significant portion of the IFN-associated response. Murine embryonic fibroblasts (MEFs) deficient in IFITM3 were more readily infected with influenza virus before and particularly after treatment with IFNα when compared with wild type (WT) MEFs (8). Likewise, IFITM3 knock-out mice and humans possessing specific IFITM3 gene mutations are more susceptible to disease caused by influenza virus (9). In addition, overexpression studies have shown that IFITM3 also inhibits many other pathogenic viruses including hepatitis C virus, dengue virus, West Nile virus, vesicular stomatitis virus, human immunodeficiency virus (HIV), and severe acute respiratory syndrome (SARS) virus (7, 8, 10–13). A commonality among IFITM3-inhibited viruses has emerged in that all of these viruses are able to enter cells via endocytosis. Likewise, the multitude of viruses that are inhibited and the variability in their individual proteins suggests that a general mechanism rather than a direct IFITM3/virus protein interaction mediates antiviral activity.

The molecular mechanism by which IFITMs restricts virus infection is still unclear, but additional experiments have suggested that the most active isoform, IFITM3, does not block the binding or entry of vesicular stomatitis virus (12), influenza virus (11, 14), or hepatitis C virus (7) into host cells but prevents deposition of viral contents into the cytosol (14). IFITM3 expression has also been described to expand acidic cellular compartments (11) that stain positive for endolysosomal and autophagosomal markers, LAMP1, Rab7, and LC3 (14). Interestingly, incoming influenza virus colocalizes with this acidic compartment and IFITM3 and is eliminated by 6 h post-infection. These observations suggest that IFITM3 induces a degradative compartment unique from the acidified endosomes

* This work was supported, in whole or in part, by National Institutes of Health Grants 1K99AI095348 (NIAID; to J. S. Y) and 1R01GM087544 (NIGMS'; to H. C. H.). This work was also supported by the Ellison Medical Foundation (to H. C. H.).
[S] This article contains supplemental Table 1 and Figs. 1–7.
[1] To whom correspondence should be addressed. Tel.: 212-327-7275; Fax: 212-327-7276; E-mail: hhang@rockefeller.edu.

[2] The abbreviations used are: IFITM, IFN-induced transmembrane; MEF, murine embryonic fibroblast; az-Rho, azido-rhodamine; ATG5, autophagy protein 5; ER, endoplasmic reticulum; NP, nucleoprotein.

where viruses typically fuse with host membranes to deliver their contents into the cytosol for replication (14).

Our previous palmitoylome profiling studies revealed that IFITM3 is *S*-palmitoylated on three membrane proximal cysteine resides (10). An IFITM3 mutant lacking all three *S*-palmitoylation sites exhibited a more diffuse cellular staining pattern and significantly diminished antiviral activity, suggesting that correct membrane positioning of IFITM3 is critical for its function (10). Here we demonstrate that IFITM3 is also ubiquitinated on conserved lysine residues that are important for regulating its stability, endolysosomal localization/alteration, and antiviral activity. The mapping of IFITM3 ubiquitination sites also challenged its predicted membrane topology and revealed that the N and C termini of IFITM3 are predominantly oriented toward the cytosol. Our results collectively suggest that IFITM3 is an intramembrane protein that is targeted to endocytic vesicles by *S*-palmitoylation in the absence of ubiquitination. Both of these posttranslational modifications strongly regulate the antiviral activity of IFITM3 and have provided new insight into its mechanism of action.

EXPERIMENTAL PROCEDURES

Cell Culture, Transfections, and Western Blots—HeLa cells, HEK293T cells, HEK293 cells stably expressing GFP-LC3 (provided by Sharon Tooze, Cancer Research UK), DC2.4 cells, and WT and ATG5$^{-/-}$ MEFs (provided by Noboru Mizushima, Tokyo Medical and Dental University) (15) were grown in DMEM supplemented with 4.5 g/liter D-glucose, 110 mg/liter sodium pyruvate, and 10% FBS (Gemini Bio-Products) at 37 °C in a humidified incubator with an atmosphere of 5% CO_2. Cellular fractionation experiments were performed using freshly harvested cells and the Qiagen Qproteome Cell Compartment Kit followed by acetone precipitation and loading of 20 μg of protein per lane for SDS-PAGE. For microscopy experiments, cells were grown in 12-well plates on glass coverslips to ~50% confluence and transfected with 1 μg of the indicated plasmids per well using Lipofectamine 2000 (Invitrogen). For Western blotting, cells were grown on 6-well plates to ~90% confluence and transfected with 2 μg of the indicated plasmids per well using Lipofectamine 2000. The pCMV-HA-IFITM3 construct has been described previously (10) Primers for generation of HA-IFITM3-PalmΔ were previously described (10), and primers used to generate IFITM3 lysine mutants, the myristoylation/prenylation mutant, and glycosylation site insertion mutants are listed in supplemental Table 1. pSELECT-GFP-LC3 was purchased from Invivogen. Plasmids encoding GFP-Rab5, GFP-Rab7, and LAMP1-GFP have been previously described (16, 17) and were kindly provided by Julia Sable (The Rockefeller University, New York). For retroviral transduction of MEFs, IFITM3-HA coding sequence was cloned into pRetroX-IRES-ZsGreen1 (Clontech) using BglII and BamHI restriction sites. IFNα2 was purchased from eBioscience and used at a concentration of 0.1 μg/ml. Ambion Silencer Select predesigned and validated control and IFITM3 siRNAs were purchased from Invitrogen and were transfected into MEFs using RNAiMax transfection reagent also from Invitrogen.

For Western blotting, cells were lysed with Brij 97 buffer (1% Brij 97, 150 mM NaCl, 50 mM TEA, pH 7.4). Western blotting was performed with anti-HA antibody (Clontech, 631207) at 1:1000. For Western analysis of GFP-LC3, anti-GFP (Clontech, JL-8) at 1:1000 was used. Anti-GAPDH (Abcam, ab70699), anti-calnexin (Abcam, ab22595), anti-IFITM3 (Abcam, ab15592), and anti-ubiquitin (Covance) were also used at 1:1000 dilutions. Immunoprecipitations were performed using anti-HA-conjugated agarose (Sigma).

Infections, Fluorescence Microscopy, and Flow Cytometry—Influenza virus A/PR/8/34 (H1N1) was propagated in 10-day embryonated chicken eggs for 40 h at 37 °C and titrated using Madin-Darby canine kidney cells. Cells were infected at a multiplicity of infection of 2.5 for 6 h before fixation and staining. For *Salmonella typhimurium* infections, strain IR715 was used, and infections were performed as previously described (18). For both flow cytometry and microscopy, cells were fixed with 3.7% paraformaldehyde in PBS for 10 min followed by a 10-min permeabilization with 0.2% saponin in PBS and a 10-min blocking step with 2% FBS in PBS. Cells were stained using anti-HA anti-antibody (Covance, clone 16B12) directly conjugated to Alexa-488, -555, or -647 using kits for 100 μg of antibody available from Invitrogen. Anti-NP (Abcam, ab20343) was directly conjugated to Alexa-647 using a similar kit. Likewise, anti-myc (Clontech, 631206) was conjugated to Alexa-488. All conjugated antibodies were used at a 1:200 dilution in 0.2% saponin in PBS for 30 min at room temperature for both microscopy and flow cytometry. Anti-calreticulin (Abcam, ab2907) was used at a 1:1000 dilution followed by a goat anti-rabbit secondary conjugated to Alexa-488 (Invitrogen). TOPRO-3 (Invitrogen) was used at a 1:1000 dilution in PBS for 10 min to stain nuclei as a final step in some experiments before glass slide mounting in ProLong Gold Antifade Reagent (Invitrogen).

Metabolic Labeling with Chemical Reporters and MS/MS—Cells were metabolically labeled for 2 h with 50 μM alk-16 or for 4 h with alk-12 or alk-FOH in DMEM supplemented with 2% charcoal filtered fetal bovine serum (Omega Scientific). Cells were lysed with 1% Brij buffer (0.1 mM triethanolamine, 150 mM NaCl, 1% Brij97, pH 7.4) containing EDTA-free protease inhibitor mixture (Roche Applied Science). Proteins were immunoprecipitated and subjected to click chemistry reactions containing 100 μM azido-rhodamine (az-Rho), 1 mM tris(2-carboxyethyl)phosphine hydrochloride (TCEP), 100 μM tris[(1-benzyl-1*H*-1,2,3-triazol-4-yl)methyl]amine (TBTA), and 1 mM $CuSO_4 \cdot 5H_2O$. In-gel fluorescence scanning was performed using a Typhoon 9400 imager (Amersham Biosciences) (excitation 532 nm, 580-nm detection filter).

LC-MS/MS analysis was performed on immunoprecipitated HA-IFITM3 peptides recovered from trypsin-treated gel slices with a Dionex 3000 nano-HPLC coupled to an LTQ-Orbitrap ion trap mass spectrometer (ThermoFisher). Peptides were identified using SEQUEST Version 28 searched against the mouse (v3.45) and human (v3.56) International Protein Index (IPI) protein sequence databases with an allowance for 114 Da modifications on lysines indicative of ubiquitination. Scaffold software (Proteome Software) was used to compile data.

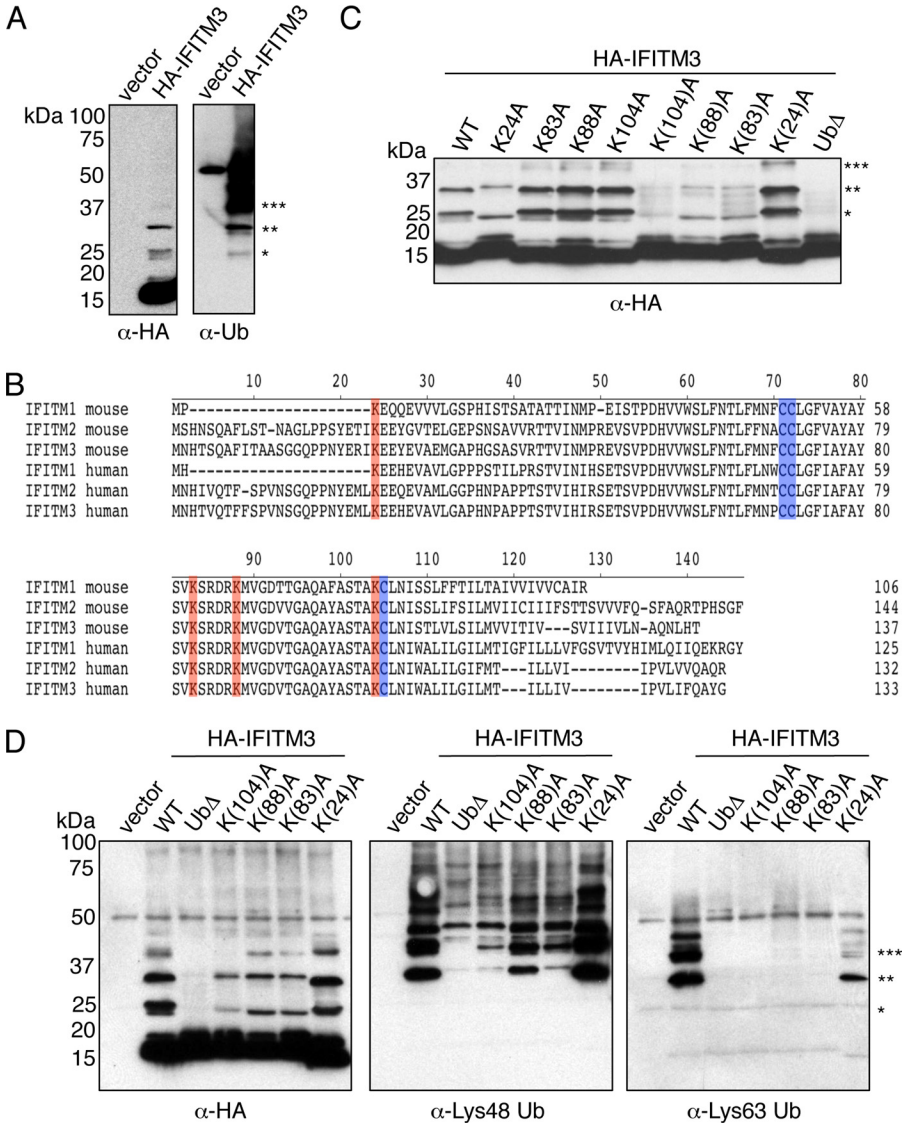

FIGURE 1. **IFITM3 is polyubiquitinated with Lys-48 and Lys-63 linkages.** *A*, *C*, and *D*, HEK293T cells were transfected overnight with the indicated plasmids. Immunoprecipitation was performed on cell lysates using α-HA agarose. *A*, Western blotting was performed using α-HA and α-ubiquitin (*Ub*) antibodies. *B*, shown is alignment of human and mouse IFITM isoforms 1–3 using the ClustalV method. Conserved palmitoylated cysteines are highlighted in *blue*, and conserved lysines are *shaded red*. *C*, Western blotting was performed using α-HA antibodies to visualize IFITM3 and ubiquitinated species. *D*, Western blotting was performed using α-HA antibodies and antibodies specifically recognizing Lys-48- or Lys-63-linked ubiquitin chains (α-Lys-48 Ub and α-Lys-63 Ub). *A*, *C*, and *D*, *asterisks* indicate modification with one, two, or three ubiquitin molecules. *C* and *D*, *parentheses* indicate the one lysine of four that is not mutated to alanine. *Ub*Δ indicates mutation of Lys-24, Lys-83, Lys-88, and Lys-104 to alanine.

RESULTS

IFITM3 Is Polyubiquitinated with Lys-48 and Lys-63 Linkages—Although IFITM3 has a predicted molecular mass of 15 kDa, Western blot analysis showed additional higher molecular mass IFITM3-specific bands (Fig. 1*A*). Large scale immunoprecipitation of murine HA-tagged IFITM3 (HA-IFITM3) and mass spectrometry sequencing of the recovered peptides from trypsin-digested gel slices revealed that these upper bands were indeed IFITM3. Ubiquitin was also selectively identified in the upper bands (supplemental Fig. 1*A*), and one site of HA-IFITM3 ubiquitination was revealed on lysine 24 (supplemental Fig. 1*B*). Anti-ubiquitin Western blot analysis of immunoprecipitated HA-IFITM3 further confirmed that IFITM3 is modified with one, two, and three ubiquitin molecules and is also polyubiquitinated (Fig. 1*A*). Higher molecular weight IFITM3 species and positive anti-ubiquitin blots were also seen for endogenous IFITM3 immunoprecipitated from MEFs and DC2.4 cells (supplemental Fig. 1*C*). Confirming these observations, two recent global proteomic studies of ubiquitinated proteins also identified ubiquitinated peptides from endogenous IFITM3 (19, 20).

Sequence alignment of IFITM isoforms revealed that Lys-24 and three other lysine residues are highly conserved (Fig. 1*B*). As our mass spectrometry analysis did not preclude ubiquitination at lysines other than Lys-24, we generated individual lysine mutants as well as IFITM3 mutants in which three of the four lysines or all four lysines (*Ub*Δ) were mutated to alanine. The analysis of these IFITM3 lysine mutants after immunoprecipitation revealed that ubiquitination is most prevalent on Lys-24 but can also occur on Lys-83, Lys-88, and Lys-104 (Fig. 1*C*). The

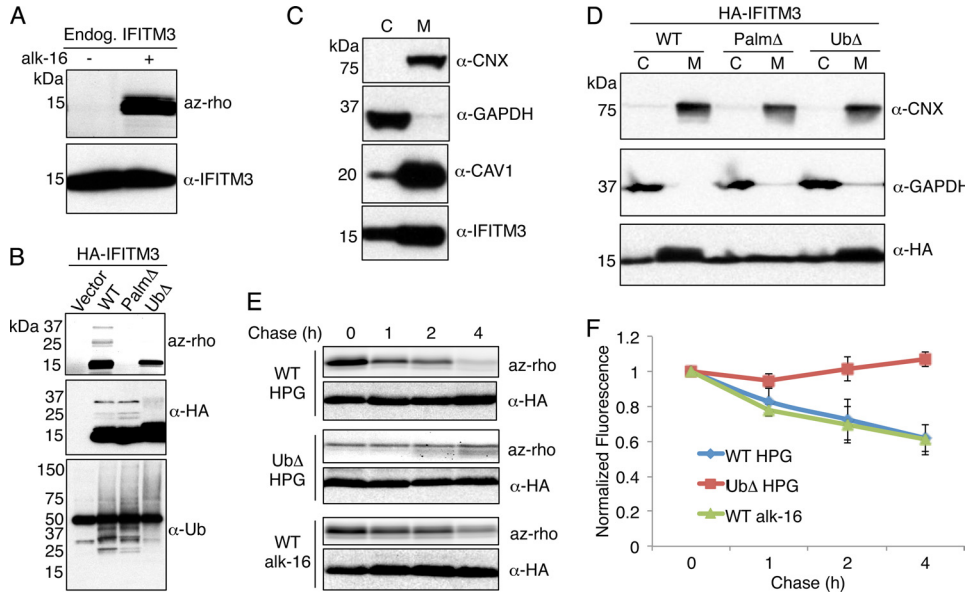

FIGURE 2. **Ubiquitination and *S*-palmitoylation of IFITM3 have distinct roles.** *A*, MEFs were treated for 6 h with IFNα before an additional 2 h treatment with IFNα and alkynyl palmitic acid reporter, alk-16, at 50 μM or DMSO as a control. Immunoprecipitated IFITM3 was reacted with az-rho via click chemistry and was visualized by fluorescence gel scanning and α-IFITM3 Western blotting. *B*, *D*, *E*, and *F*, HEK293T cells were transfected overnight with the indicated plasmids. *Palm*Δ indicates mutation of Cys-71, Cys-72, and Cys-105 to alanine. *Ub*Δ indicates mutation of Lys-24, Lys-83, Lys-88, and Lys-104 to alanine. *B*, transfected cells were labeled with alkynyl-palmitic acid reporter, alk-16, for 2 h at 50 μM. Immunoprecipitated proteins were reacted with az-rho via click chemistry and visualized by fluorescence gel scanning and α-HA Western blotting. MEFs treated with IFNα for 8 h (*C*) or transfected cells (*D*) were fractionated into membrane and cytosolic compartments. α-Calnexin (*CNX*), α-GAPDH, and α-caveolin-1 (*CAV1*) Western blotting provided membrane, cytoplasmic, and intramembrane controls, respectively, for blotting with α-IFITM3 or α-HA antibodies. *E*, transfected cells were labeled with homopropargylglycine (*HPG*; 250 mM) or alk-16 (50 μM) for 2 h followed by chase with media containing either 5 mM methionine or 100 μM palmitate, respectively, for the indicated times. Immunoprecipitated proteins were reacted with az-rho via click chemistry and visualized by fluorescence gel scanning and α-HA Western blotting. *F*, shown are the average results from four experiments performed as in *D*. Fluorescence signal was normalized to Western blots to control for protein loading, and values were plotted relative to 0 h of chase. *Error bars* represent S.E.

complete loss of ubiquitinated bands visualized by Western blotting could only be achieved when all four lysines were mutated to alanine (Fig. 1*C*). The analysis of lysine mutants using polyubiquitin linkage-specific antibodies showed that IFITM3 is ubiquitinated with Lys-48 linkages on all four lysine residues and most robustly on Lys-24 (Fig. 1*D*). IFITM3 is also polyubiquitinated with Lys-63 linkages on Lys-24 and possibly other lysines in the wild type protein (Fig. 1*D*).

Ubiquitination and S-Palmitoylation Regulate Distinct Aspects of IFITM3 Activity—Extending our previous observation that HA-tagged IFITM3 constructs are *S*-palmitoylated, we utilized metabolic incorporation of an alkynyl-palmitic acid reporter (alk-16) followed by click chemistry labeling with az-rho and in-gel fluorescence detection to show that endogenous IFITM3 produced in IFNα-treated MEFs is palmitoylated (Fig. 2*A*). Next, we examined potential interplay between palmitoylation and ubiquitination. Alk-16 labeling and fluorescence gel scanning along with Western blotting showed that *S*-palmitoylation of IFITM3 can occur independently of ubiquitination (Fig. 2*B*). Similarly, IFITM3 deficient in *S*-palmitoylation (PalmΔ) (10) was effectively ubiquitinated (Fig. 2*B*), and IFITM3 that is both ubiquitinated and *S*-palmitoylated can be visualized by fluorescence gel scanning (Fig. 2*B*). Thus, these modifications occur independently and are not mutually exclusive.

Membrane fractionation of IFNα-treated MEFs revealed that endogenous IFITM3 partitions to both cytoplasmic and membrane fractions, unlike calnexin, a known transmembrane protein, but like caveolin-1, which is well characterized to be an intramembrane protein partially localized to the cytosol (21, 22) (Fig. 2*C*). Similarly, in HEK293T cells, we observed that HA-IFITM3 is primarily membrane-associated but is also present in cytoplasmic fractions at lower levels (Fig. 2*D*). HA-IFITM3-UbΔ behaved similarly to HA-IFITM3, whereas the PalmΔ mutant showed less partitioning into the membrane fraction compared with WT protein (Fig. 2*D*). These data demonstrate that IFITM3 has an inherent affinity for cellular membranes that is ubiquitin-independent, but the addition of hydrophobic *S*-palmitoylation enhances its membrane partitioning.

Given our detection of IFITM3 modification by Lys-48-linked polyubiquitin and that this is often associated with proteasomal degradation, we analyzed turnover of wild type and ubiquitination-deficient IFITM3. We took advantage of a non-radioactive pulse-chase method utilizing an alkynyl methionine surrogate, homopropargylglycine, and detection of labeled protein through click chemistry reaction with az-rho followed by in-gel fluorescence scanning. We found that although wild type HA-IFITM3 signal decayed during the 4-h chase period, HA-IFITM3-UbΔ signal was relatively stable (Fig. 2, *E* and *F*). Interestingly, significantly less homopropargylglycine was incorporated into the UbΔ mutant compared with wild type, indicating that its relative synthesis is slowed (Fig. 2*E*). This is in agreement with similar overall levels of WT IFITM3 and UbΔ mutant being present in cells as measured by Western blotting and flow cytometry (supplemental Fig. 2, *A* and *B*) and may suggest that a feedback mechanism exists regulating IFITM3 translation. Thus, although ubiquitination regulates IFITM3

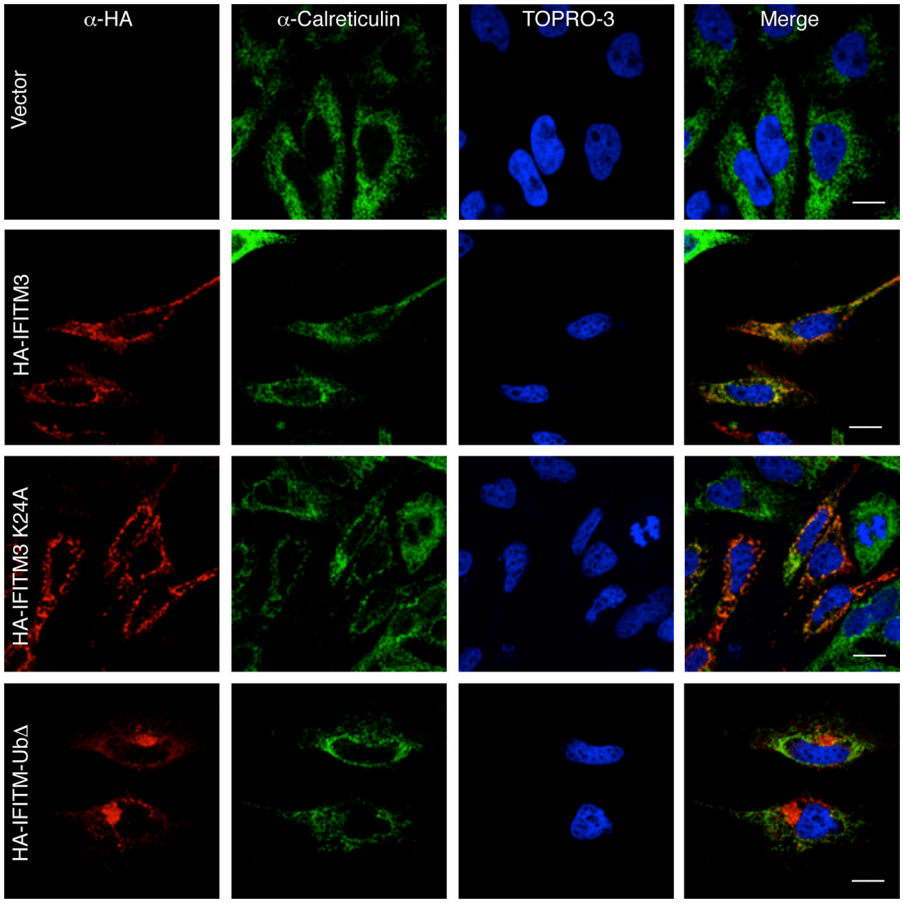

FIGURE 3. **Ubiquitination affects IFITM3 localization.** HeLa cells were transfected overnight with empty vector or plasmids encoding the indicated IFITM3 constructs. Immunofluorescence with α-HA antibodies allowed IFITM3 visualization, and α-calreticulin staining allowed visualization of the ER. TOPRO-3 was used to visualize nuclei. *Scale bars* indicate 10 μm. *Ub*Δ indicates mutation of Lys-24, Lys-83, Lys-88, and Lys-104 to alanine.

stability, the UbΔ mutant is not observed at higher levels than wild type protein. Concurrent with these protein stability assays, we also performed a pulse-chase experiment using alk-16 to determine whether *S*-palmitoylation of IFITM3 is dynamic or irreversible. Interestingly, decay of alk-16-dependent signal was nearly identical to the turnover of wild type protein, suggesting that *S*-palmitoylation on IFITM3 is likely stable (Fig. 2*F*).

Non-ubiquitinated IFITM3 Localizes to Endolysosomal Compartments and Has Increased Antiviral Activity—Because ubiquitination, particularly Lys-63-linked ubiquitin chains, can control protein trafficking, we also evaluated the cellular localization of the IFITM3 ubiquitination mutant. We first analyzed IFITM3 along with the ER protein, calreticulin, based on our previous costaining studies with this marker (10) and other reports of ER localization (8). Lysine mutants of HA-IFITM3 colocalized with calreticulin similarly to wild type HA-IFITM3, as represented by HA-IFITM3 K24A (Fig. 3). In contrast, HA-IFITM3-UbΔ showed a distinct distribution to a perinuclear site away from calreticulin positive regions (Fig. 3). As human IFITM3 has also been reported to induce enlarged acidified compartments that stain positive for endolysosomal markers (14), we evaluated whether ubiquitinated lysines influence HA-IFITM3 targeting to these compartments. Indeed, GFP-tagged LAMP1, Rab7, and Rab5 showed partial colocalization with HA-IFITM3 that was dramatically enhanced with HA-IFITM3-UbΔ (Fig. 4*A* and supplemental Fig. 3). This colocalization is specific to a subset of endocytic markers as GFP-CD9 showed some colocalization with IFITM3 but did not significantly redistribute upon HA-IFITM3-UbΔ expression (Fig. 4*A* and supplemental Fig. 3). Interestingly, the distribution and clustering of GFP-LC3, a marker of autophagosomes/autolysosomes, was significantly altered by HA-IFITM3 and more so by the UbΔ mutant (Fig. 4*A* and supplemental Fig. 3), suggesting engagement of the autophagy pathway by IFITM3. These results are consistent with previous studies with human IFITM3 (14) and suggest that non-ubiquitinated IFITM3 exhibits enhanced localization with LAMP1, Rab7, and Rab5 and possesses a stronger ability to induce LC3 clustering. Similarly to transfected IFITM3, endogenous IFITM3 in MEFs also localized with this panel of endolysosomal markers (Fig. 3*B* and supplemental Fig. 4).

As IFITM3 has been shown to inhibit the influenza virus infection process before virus/endosome fusion (14), antiviral activity is determined by comparing rates of infection for control cells and cells either knocked down in IFITM3 expression or overexpressing IFITM3 constructs (8–11). Infection rates are assessed using quantitative methods such as flow cytometry and staining with virus protein-specific antibodies. The analysis of IFITM3 mutants deficient in *S*-palmitoylation or ubiquitination for activity against H1N1 influenza virus (type A, PR8 strain) infection confirmed that HA-IFITM3-PalmΔ has

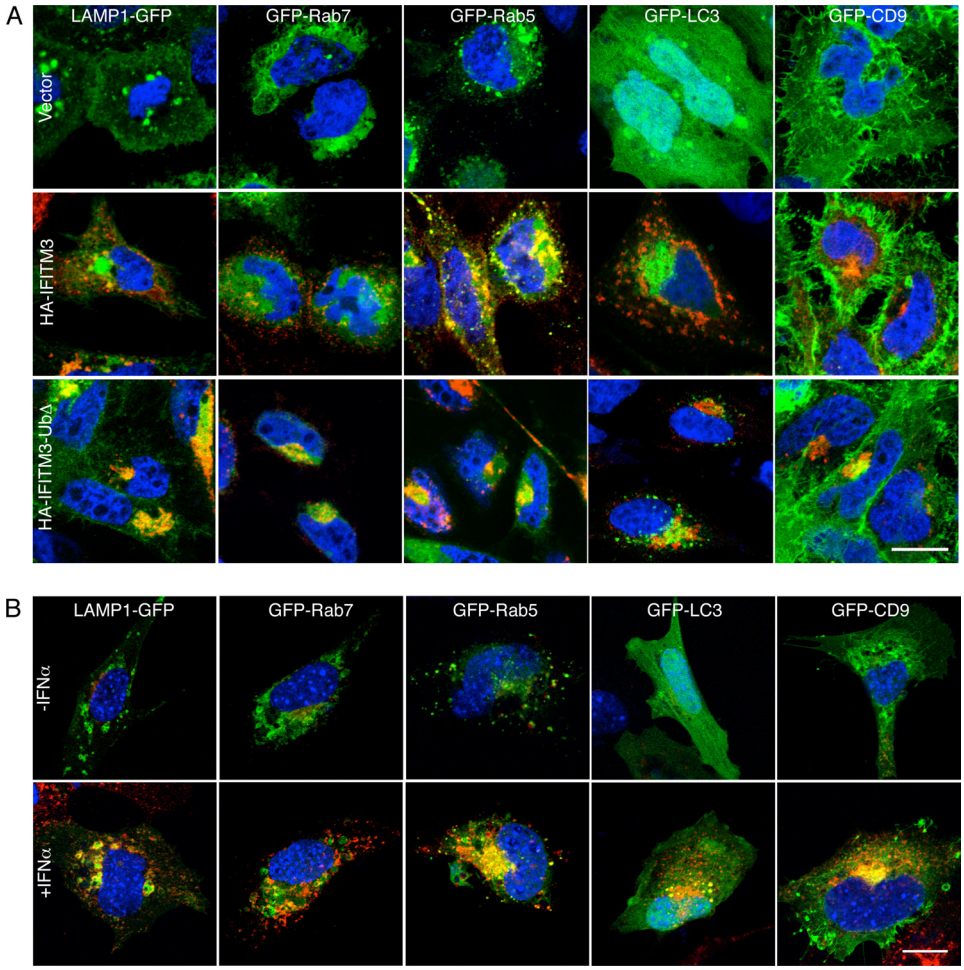

FIGURE 4. **Non-ubiquitinated IFITM3 localizes with endocytic and lysosomal markers.** *A*, HeLa cells were transfected with empty vector or plasmids encoding HA-IFITM3 or HA-IFITM3-UbΔ along with the indicated GFP-tagged protein constructs. Immunofluorescence with α-HA antibodies allowed IFITM3 visualization (*red*), whereas GFP fluorescence was used to visualize endocytic proteins (*green*), and TOPRO-3 was used to visualize nuclei (*blue*). *Ub*Δ indicates mutation of Lys-24, Lys-83, Lys-88, and Lys-104 to alanine. The *scale bar* indicates 10 μm. *B*, MEFs were transfected overnight with the indicated GFP-tagged protein constructs, and media were replaced with or without 0.1 μg/ml IFNα for 8 h. Immunofluorescence was performed with α-IFITM3 antibodies (*red*). GFP fluorescence was used to visualize endocytic proteins (*green*), and DAPI was used to visualize nuclei (*blue*). The *scale bar* indicates 10 μm.

decreased activity and revealed enhanced antiviral activity of IFITM3-UbΔ compared with HA-IFITM3 (Fig. 5). The increased antiviral activity of the UbΔ mutant was less pronounced on the PalmΔ mutant background (*Ub*Δ/*Palm*Δ, Fig. 5) indicating that membrane interaction is still crucial even for non-ubiquitinated IFITM3. Thus, *S*-palmitoylation and ubiquitination provide opposing regulation of IFITM3 activity, and taken together our data suggest that IFITM3 targeting to the endolysosomal membrane is a critical determinant of antiviral potency.

IFITM3 Induction of Autophagy Is Not Required for Anti-influenza Virus Activity—Clustering of LC3 as seen in Fig. 4 upon expression of IFITM3 is a hallmark of autophagy induction (23). We confirmed that HA-IFITM3 expression indeed induces the phosphatidylethanolamine modification of GFP-LC3 that enhances its clustering upon induction of autophagy and appears as a faster migrating band upon analysis by SDS-PAGE (Fig. 6*A*). Likewise, the lipidated form of LC3 could be elevated by the addition of chloroquine, indicating that autophagic flux, *i.e.* maturation of IFITM3-induced autophagosomes, is occurring (Fig. 6*A*). We thus hypothesized that virus particles may be targeted to IFITM3-induced autophagosomes for degradation and sought to determine whether or not the canonical autophagy protein 5 (ATG5)-dependent pathway is required for antiviral activity. To this end, we utilized ATG5$^{-/-}$ MEFs that do not show lipidation of GFP-LC3 upon HA-IFITM3 expression (supplemental Fig. 5*A*) and clustering of GFP-LC3 is drastically diminished even upon expression of HA-IFITM3-UbΔ (supplemental Fig. 5*B*). To test for antiviral activity, we targeted IFITM3 with siRNA in ATG5$^{+/+}$ and ATG5$^{-/-}$ MEFs (Fig. 6*B*). Knockdown of IFITM3 resulted in increased infection rates for both WT and ATG5$^{-/-}$ MEFs, indicating that ATG5-dependent autophagy is not required for IFITM3 anti-influenza virus activity (Fig. 6*C*). To further confirm this finding, we overexpressed IFITM3 in WT and ATG5$^{-/-}$ cells. Agreeing with our knockdown data, overexpression of IFITM3 resulted in a decreased infection rate for both WT and ATG5$^{-/-}$ cells (Fig. 6*D*). Similarly, both cell types responded normally in terms of decreased infection when treated with IFNα (Fig. 6*D*), and alteration of the GFP-LAMP1-positive compartment could still be observed in ATG5$^{-/-}$ MEFs expressing HA-IFITM3-UbΔ (Fig. 6*E*). These results demon-

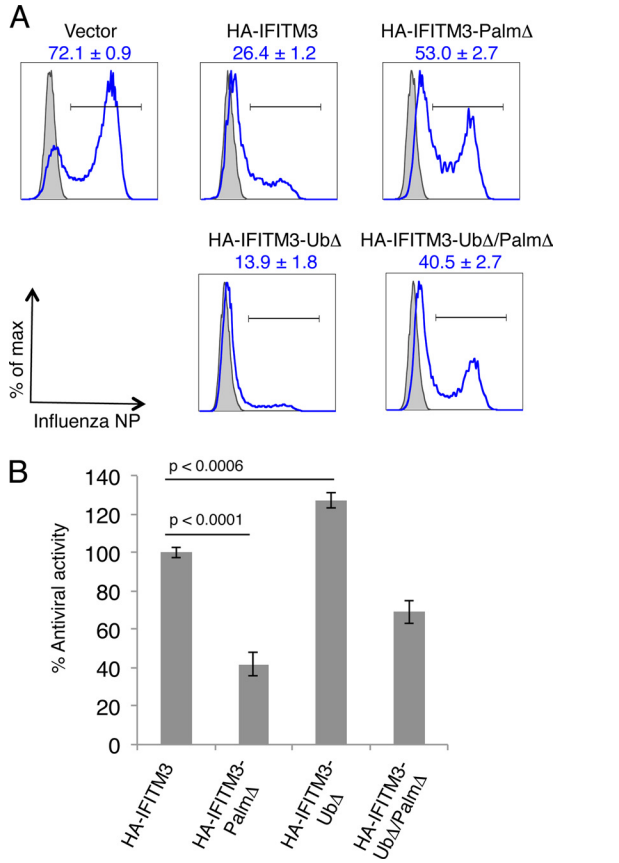

FIGURE 5. **Ubiquitination negatively regulates antiviral activity of IFITM3.** *A* and *B*, HEK293T cells were transfected overnight with indicated plasmids before a 6-h infection with influenza virus at a multiplicity of infection of 2.5 and analyzed by flow cytometry. *Palm*Δ indicates mutation of Cys-71, Cys-72, and Cys-105 to alanine. *Ub*Δ indicates mutation of Lys-24, Lys-83, Lys-88, and Lys-104 to alanine. *A*, cells expressing IFITM3 constructs were analyzed for the percentage of cells that were infected using influenza-specific anti-NP antibodies. *B*, antiviral activity was calculated based on the difference in percentage of infection in HA-IFITM3-positive cells compared with vector control with this value set at 100% antiviral activity. *Error bars* represent the S.D. of triplicate samples. *p* values were determined using Student's *t* test. Data are representative of more than five experiments.

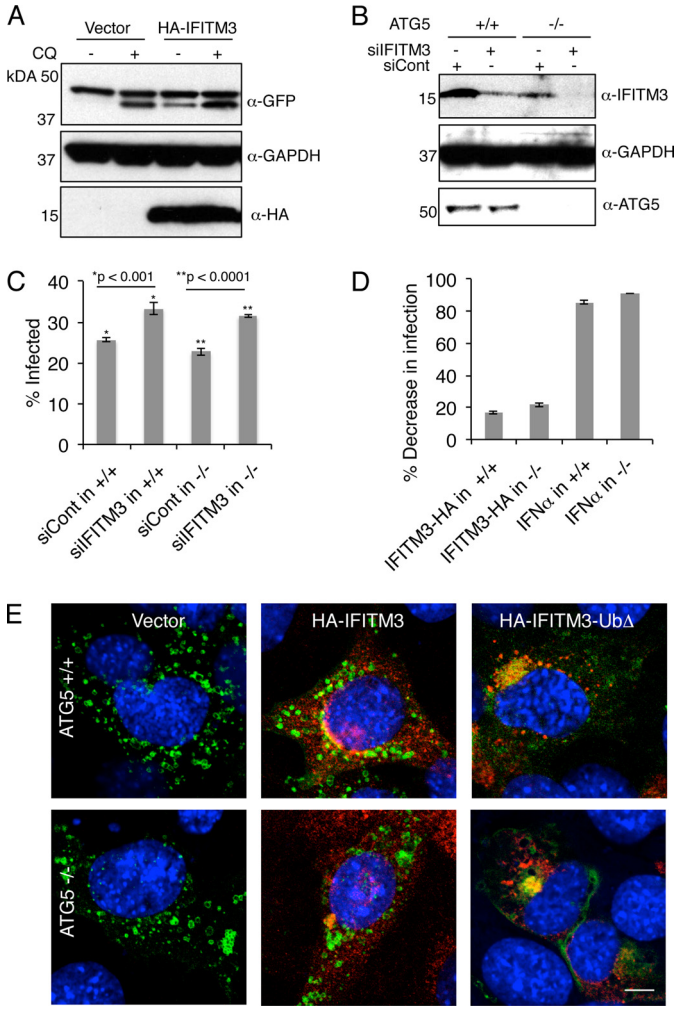

FIGURE 6. **IFITM3 antiviral activity is not dependent on induction of autophagy.** *A*, HEK293T cells stably expressing GFP-LC3 were transfected overnight with vector control or HA-IFITM3. Cells were then treated with chloroquine (*CQ*) at 40 μM or DMSO for 2 h. Cell lysates were analyzed by Western blotting with α-HA, α-GFP, and α-GAPDH antibodies. *B* and *C*, $ATG5^{+/+}$ or $ATG5^{-/-}$ MEFs were treated with control siRNA or siRNA targeting IFITM3 for 24 h. *B*, cell lysates were analyzed by Western blotting with α-IFITM3, α-GAPDH, and α-ATG5. *C*, siRNA-treated cells were infected with influenza virus at a multiplicity of infection of 2.5 for 6 h and analyzed by flow cytometry for the percentage of infected cells. *p* values were determined using Student's *t* test. Results are representative of at least three experiments. *D*, $ATG5^{+/+}$ or $ATG5^{-/-}$ MEFs expressing IFITM3-HA were infected with influenza virus at a multiplicity of infection of 2.5 for 6 h and analyzed by flow cytometry for the percentage of infected cells. Infection decrease is relative to control cells expressing ZsGreen. Alternatively, wild type or knock-out cells were treated with IFNα for 6 h before infection and analyzed by flow cytometry for the percentage of infected cells. Decreased infection is relative to untreated cells. Results are representative of two experiments. *E*, $ATG5^{+/+}$ or $ATG5^{-/-}$ MEFs were transfected with LAMP1-GFP and the indicated IFITM3 constructs. Immunofluorescence with α-HA antibodies allowed IFITM3 visualization (*red*), whereas GFP fluorescence was used to visualize LAMP1 (*green*), and TOPRO-3 was used to visualize nuclei (*blue*). The *scale bar* indicates 10 μm.

strate that ATG5-dependent autophagy is not required for IFITM3 antiviral activity.

We next hypothesized that IFITM3, particularly its regulation of the endolysosomal pathway, might offer resistance to another intracellular pathogen, *S. typhimurium*. We thus examined *Salmonella* infection levels in MEFs treated with control or IFITM3 siRNA by flow cytometry. Although influenza infection was significantly enhanced by the IFITM3 siRNA treatment when examined at 10 h post-infection, no increase in *Salmonella* staining was observed at either 1 or 10 h post-infection (supplemental Fig. 6). This demonstrated that neither entry nor replication of *Salmonella* is restricted by IFITM3 in MEFs. Overall, these results indicate that changes in the endolysosomal pathway induced by IFITM3 specifically inhibit virus infection and not entry or replication of the intracellular bacteria *S. typhimurium*.

IFITM3 Is an Intramembrane Protein—IFITM3 is proposed to be a dual-pass transmembrane protein with N and C termini both facing the lumen of the ER or endolysosome (8, 10, 11, 14). However, this topology model has not been conclusively established, nor is it consistent with observations regarding IFITM3 biochemistry and localization. Several observations led us to challenge the predicted topology of IFITM3. 1) Ubiquitination of IFITM3 at Lys-24 (Fig. 1, *A*, *C*, and *D*) is not consistent with its N-terminal lumenal orientation, as ubiquitin-conjugating enzymes are only reported in the cytoplasm. 2) IFITM3 possesses two glycosylation motifs (Fig. 1*B*), one being at the N terminus predicted to be lumenally localized, yet there has been

no report of IFITM3 glycosylation in the ER. 3) Several IFITM isoforms in various species have truncated C termini that would not support a complete transmembrane domain or have a C-terminal C*AAX* motif that would suggest cytoplasmic prenylation (24) (Fig. 1*B*). 4) Membrane fractionation of IFITM3 indicates that it is partially cytoplasmic and likely not a true transmembrane protein (Fig. 2, *C* and *D*). 5) IFITM3 N-terminal tags can be colocalized with lysosomal compartments (Figs. 4*A* and 6*E*), and HA-IFITM3 levels are not increased by inhibiting lysosomal acidification (Fig. 6*A*), suggesting that this non-glycosylated protein is protected from degradation by facing the cytoplasm rather than the lysosome lumen.

To evaluate the membrane protein topology of IFITM3 we generated several constructs with *N*-linked glycosylation sites in different regions of the protein for potential modification by ER resident enzymes. Upon confirmation that WT IFITM3 is indeed not glycosylated (Fig. 7*B*), we then engineered additional *N*-linked glycosylation sites at the N terminus (S38N), predicted cytoplasmic loop (D92N), and C terminus (H136T). Treatment of immunoprecipitated HA-IFITM3 with peptide *N*-glycosidase F had no effect on the mobility of IFITM3 regardless of the mutant tested, whereas a control protein, HA-tagged mannose 6-phosphate receptor, known to be glycosylated, showed a band collapse upon digestion of *N*-linked glycans (Fig. 7*B*). Each of the glycosylation site insertion mutants showed antiviral activity similar to WT IFITM3, demonstrating these constructs are active and not significantly perturbed in function (Fig. 7*C*). Thus, *N*-linked glycosylation site insertion analysis does not support the predicted topology or an inversion of the predicted topology but would be consistent with a cytoplasmic-facing intramembrane topology (Fig. 7*A*).

In addition to accessibility of the IFITM3 N terminus to cytoplasmic ubiquitin ligases (Fig. 1, *A*, *C*, and *D*), we sought to confirm that indeed both ends of the molecule were accessible to cytoplasmic enzymes while retaining activity. We reasoned that insertion of an N-terminal myristoylation motif and C-terminal C*AAX* box would allow us to assess accessibility of the termini to cytoplasmic myristoyl and prenyl transferases, respectively (Fig. 7*A*). Concurrently, if modified, these irreversible lipid modifications would tether the protein ends to the cytoplasmic face of the membrane bilayer similar to the alternative topology we propose (Fig. 7*A*). We thus added an N-terminal glycine-containing myristoylated motif from the HIV gag protein (GARASVLS) as well as a C-terminal prenylation site from RhoA (CLVL) to our *S*-palmitoylation-deficient HA-IFITM3 construct. Using chemical reporters developed and validated for the study of myristoylation (alk-12) (25, 26) and prenylation (alk-FOH) (27, 28), we confirmed that the G-HA-IFITM3-PalmΔ-CLVL construct is both myristoylated and prenylated (Fig. 7*D*). This construct maintained calreticulin colocalization (supplemental Fig. 7) similarly to wild type IFITM3 (Fig. 3). Importantly, the diffuse staining reported for HA-IFITM3-PalmΔ (10) was not observed, and G-HA-IFITM3-PalmΔ-CLVL showed largely overlapping localization when compared with a myc-tagged WT IFITM3 (Fig. 7*E*). Likewise, in membrane fractionation assays, these irreversible lipid modifications rescued the membrane partitioning of the PalmΔ mutant to a membrane:cytoplasmic ratio similar to the WT protein (Fig. 7*F*). We next tested whether the tethering of the N and C termini to the cytoplasmic face of the membrane would affect antiviral activity and discovered that these modifications also rescued the anti-influenza virus activity of the PalmΔ mutant (Fig. 7*G*). Thus both termini of active IFITM3 face the cytoplasm and the inherent membrane affinity of IFITM3 is likely due to intramembrane domains rather than transmembrane domains as had been postulated.

DISCUSSION

The characterization of IFITM3 *S*-palmitoylation and ubiquitination reveals important modes of posttranslational regulation and provides further insight into the mechanism of antiviral activity for this family of IFN effectors. Our discovery of IFITM3 ubiquitination (Fig. 1) and analysis of a ubiquitination-deficient mutant (Figs. 4 and 5) provide support for a model in which virus infection is restricted by an alteration of the endolysosomal compartment and reveal a novel layer of regulation for this antiviral process. The lysine-less mutant of IFITM3 exhibits enhanced localization with endolysosomal markers (Figs. 3 and 4) and increased antiviral activity associated with enhanced rearrangement of this compartment (Fig. 5). The possibility also remains that modifications in addition to ubiquitination, such as lysine acetylation or a lysine-based sorting signal, may contribute to the antiviral activity of IFITM3. *S*-Palmitoylation-deficient IFITM3 has a distinct phenotype with decreased membrane affinity and dampened activity (Figs. 1 and 5) (10). These results suggest that non-ubiquitinated and *S*-palmitoylated IFITM3 represent the most active protein population for sequestration and degradation of incoming virus particles.

The discovery of IFITM3 ubiquitination may also resolve some conflicting observations and raises interesting questions regarding protein to vesicle targeting mechanisms. Initial reports showed that IFITM3 colocalizes with ER markers (8, 10) and that it may be targeted to the plasma membrane (8), but recent studies suggest it is primarily associated with endocytic markers (11, 14). The fact that wild type IFITM3 is dually post-translationally modified and likely exists as a heterogeneous protein population may explain these potentially disparate observations. Nonetheless, our results clearly demonstrate that non-ubiquitinated and *S*-palmitoylated IFITM3 is intracellular and is enriched in endolysosomal compartments. IFITM3 has also been suggested to induce the formation of acidic autolysosomal compartments (14). Our results confirm that autophagy is indeed induced by IFITM3 expression (Figs. 4 and 6*A*), yet canonical ATG5-mediated autophagy induction is not required for IFITM3 antiviral activity (Fig. 5). Formation of autolysosomes in IFITM3-expressing cells may be a downstream effect of alterations in endolysosomes. It remains to be determined if IFITM3 plays a role in starvation or drug-induced autophagic processes.

Our data examining posttranslational modification of IFITM3 also challenge the predicted dual-pass transmembrane topology of IFITM3 in which N and C termini face into the ER and endosome/lysosome lumen (8, 12, 24). Unlike true transmembrane proteins, a portion of IFITM3 fractionates with cytoplasmic proteins and membrane association is enhanced by *S*-palmitoylation (Figs. 2, *B* and *C*, and 7*F*). This fractionation

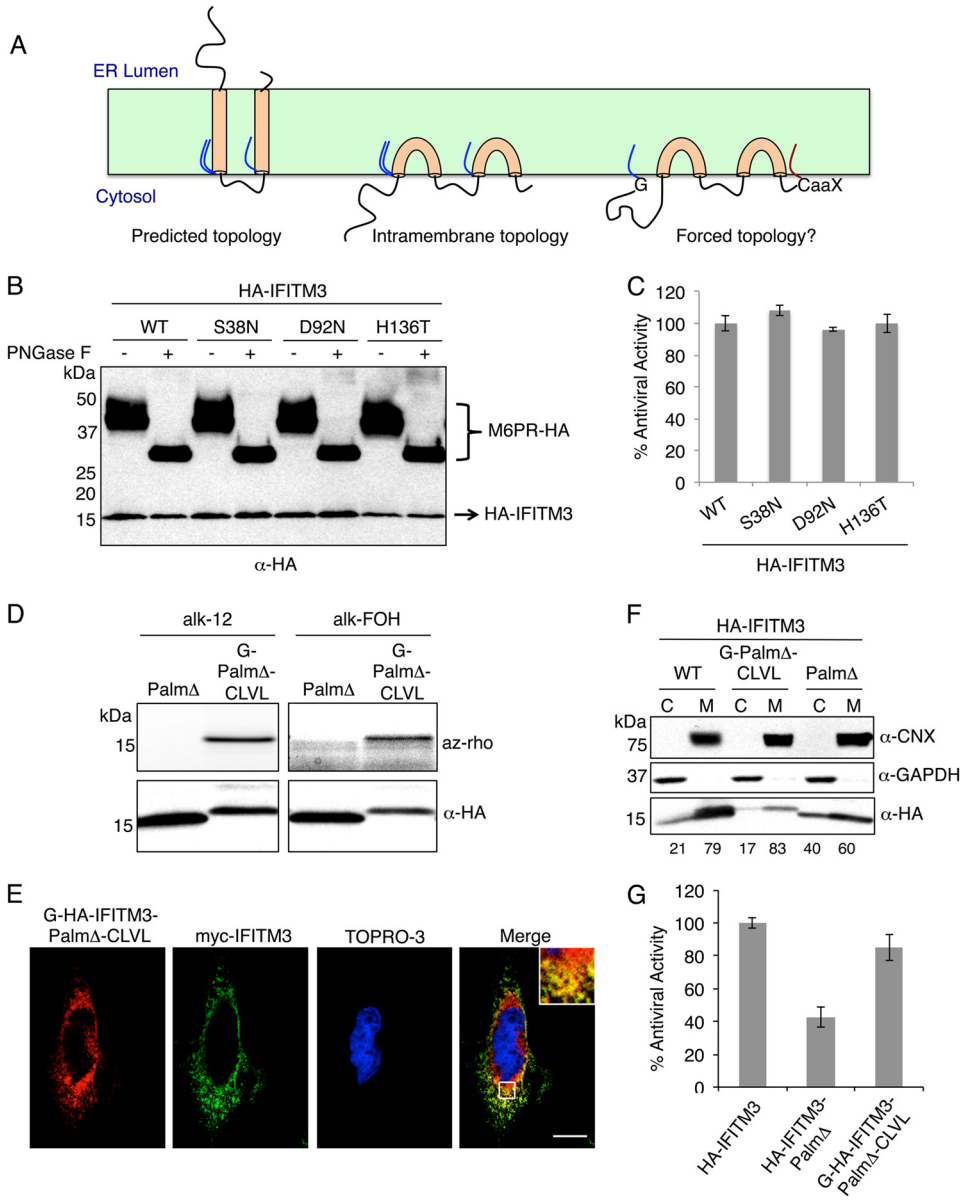

FIGURE 7. **IFITM3 is a cytoplasm-facing intramembrane protein.** *A*, potential topologies for IFITM3 or a myristoylated and prenylated IFITM3 mutant are shown. *B*, HEK293T cells were transfected with plasmid expressing HA-tagged mannose 6-phosphate receptor (*M6PR-HA*) and the indicated HA-IFITM3 constructs. HA-tagged proteins were immunoprecipitated, and samples were split in two for mock treatment or treatment with peptide *N*-glycosidase F (*PNGase F*) for 1 h. Western blotting with α-HA antibodies demonstrates that IFITM3 does not undergo a band shift characteristic of glycosylation. *C*, HEK293T cells expressing IFITM3 constructs were analyzed for the percentage of cells that were infected. Antiviral activity was calculated based on the difference in percentage of infection in HA-IFITM3-positive cells compared with vector control with this value being set at 100% antiviral activity. *D*, HEK293T cells were transfected overnight with the indicated plasmids. Cells were labeled with alkynyl-myristoylation (*alk-12*) or alkynyl prenylation (*alk-FOH*) reporters for 4 h at 50 μM. Immunoprecipitated proteins were reacted with az-rho via click chemistry and visualized by fluorescence gel scanning and α-HA Western blotting. *E*, HeLa cells were transfected with the indicated plasmids and visualized with α-HA (*red*) and α-myc (*green*) antibodies as well as TOPRO-3 (*blue*) for staining nuclei. The *scale bar* indicates 10 μm. *F*, HEK293T cells were transfected with the indicated IFITM3 constructs overnight and fractionated into cytoplasmic and membrane compartments. α-Calnexin (*CNX*) and α-GAPDH Western blotting provided membrane (*M*) and cytoplasmic (*C*) controls, respectively, for blotting with α-HA antibodies. *Numbers below the blots* indicate the percentage of HA signal in that fraction for each IFITM3 construct. *G*, HEK293T cells expressing IFITM3 constructs were analyzed for the percentage of cells that were infected. Antiviral activity was calculated based on the difference in percentage of infection in HA-IFITM3-positive cells compared with vector control with this value being set at 100% antiviral activity. *Palm*Δ indicates mutation of Cys-71, Cys-72, and Cys-105 to alanine.

pattern is similar to what has been observed for the palmitoylated intramembrane protein caveolin (21). In addition to its membrane localization, caveolin exists in a cytoplasmic heat shock protein complex that delivers cholesterol from the ER to caveolae (21). A similar complex may exist to stabilize IFITM3 hydrophobic domains in the cytoplasm. Further evidence for an alternative IFITM3 topology came from studying ubiquitination. The lumenal orientation of Lys-24 is not compatible with the cytosolic localization of the ubiquitin conjugation machinery. Analysis of IFITM3 glycosylation or lack thereof at the N terminus, central cytoplasmic region, and C terminus demonstrated that none of these domains are exposed to ER glycosylation machinery. Likewise, adding myristoylation and prenylation sites that would tether the N and C termini to the

cytoplasmic face of membranes rescued the antiviral activity of an IFITM3 palmitoylation-deficient mutant. These results support a topology model in which the protein termini are both intracellular, and membrane association occurs via intramembrane domains.

Examination of the literature regarding proteins with intramembrane domains, such as caveolins (29), reticulons (26), flotillins (30), stomatin (31), and podocin (32) also indicates that *S*-palmitoylation adjacent to these domains is a common feature, likely facilitating membrane targeting or insertion similarly to *S*-palmitoylation on IFITM3 (Fig. 2*C*). This unpredicted topology offers insight into the biology of IFITM3 and offers new hypotheses for mechanisms of antiviral action as intramembrane domains are generally associated with inducing membrane curvature through insertion into only one leaflet of the lipid bilayer, thereby producing membrane bending by virtue of the bilayer-couple effect (33). A recent bioinformatics study has suggested that IFITMs make up a larger family of proteins with dual-pass transmembrane segments than was previously appreciated (34). These authors provide a phylogenetic model indicating that IFITMs emerged in a common ancestor of choanoflagellates and metazoa likely through a horizontal gene transfer from bacteria. However, the authors of this study also propose that this ancient and expanding family of proteins be termed dispanins for their two putative transmembrane-spanning segments. Given data indicating that IFITM3 is an intramembrane protein (Fig. 7), dysspanin may be a more appropriate moniker for this family, although a nomenclature change in general is premature until the topology of additional IFITM family members can be ascertained.

IFITM3 modulation of endocytic compartments and posttranslational regulation may also be important for other potential functions of IFITM isoforms as well as immune evasion by pathogens. For example, IFITMs have been implicated in tissue development, cell survival, and oncogenesis (35–39). In particular, IFITM3 distinguishes developing germ cells from neighboring somatic cells (36) and has been used for germ line stem cell purification (40). However, the function of IFITM3 in this cell type remains mysterious as mice lacking all IFITM isoforms possess normal germ cells and are fertile (41). Additionally, some tumor types exhibit elevated levels of IFITM3 as compared with normal tissues (38, 39), but the role of IFITM3 in tumor progression is unknown. Identification of cellular pathways that modulate IFITM3 activity or posttranslational modifications may provide important insight into these areas. Finally, as the mechanisms by which IFITM3 inhibits infection and is regulated become increasingly clear, this knowledge should facilitate the discovery of pathogen immune evasion strategies and inspire the development of new antivirals.

REFERENCES

1. Müller, U., Steinhoff, U., Reis, L. F., Hemmi, S., Pavlovic, J., Zinkernagel, R. M., and Aguet, M. (1994) Functional role of type I and type II interferons in antiviral defense. *Science* **264,** 1918–1921
2. Zhang, S. Y., Boisson-Dupuis, S., Chapgier, A., Yang, K., Bustamante, J., Puel, A., Picard, C., Abel, L., Jouanguy, E., and Casanova, J. L. (2008) Inborn errors of interferon (IFN)-mediated immunity in humans. Insights into the respective roles of IFN-α/β, IFN-γ, and IFN-λ in host defense. *Immunol. Rev.* **226,** 29–40
3. Bogdan, C. (2000) The function of type I interferons in antimicrobial immunity. *Curr. Opin. Immunol.* **12,** 419–424
4. Liu, S. Y., Sanchez, D. J., and Cheng, G. (2011) New developments in the induction and antiviral effectors of type I interferon. *Curr. Opin. Immunol.* **23,** 57–64
5. Wolf, D., and Goff, S. P. (2008) Host restriction factors blocking retroviral replication. *Annu. Rev. Genet* **42,** 143–163
6. Sadler, A. J., and Williams, B. R. (2008) Interferon-inducible antiviral effectors. *Nat. Rev. Immunol.* **8,** 559–568
7. Schoggins, J. W., Wilson, S. J., Panis, M., Murphy, M. Y., Jones, C. T., Bieniasz, P., and Rice, C. M. (2011) A diverse range of gene products are effectors of the type I interferon antiviral response. *Nature* **472,** 481–485
8. Brass, A. L., Huang, I. C., Benita, Y., John, S. P., Krishnan, M. N., Feeley, E. M., Ryan, B. J., Weyer, J. L., van der Weyden, L., Fikrig, E., Adams, D. J., Xavier, R. J., Farzan, M., and Elledge, S. J. (2009) The IFITM proteins mediate cellular resistance to influenza A H1N1 virus, West Nile virus, and dengue virus. *Cell* **139,** 1243–1254
9. Everitt, A. R., Clare, S., Pertel, T., John, S. P., Wash, R. S., Smith, S. E., Chin, C. R., Feeley, E. M., Sims, J. S., Adams, D. J., Wise, H. M., Kane, L., Goulding, D., Digard, P., Anttila, V., Baillie, J. K., Walsh, T. S., Hume, D. A., Palotie, A., Xue, Y., Colonna, V., Tyler-Smith, C., Dunning, J., Gordon, S. B., GenISIS Investigators, MOSAIC Investigators, Smyth, R. L., Openshaw, P. J., Dougan, G., Brass, A. L., and Kellam, P. (2012) IFITM3 restricts the morbidity and mortality associated with influenza. *Nature* **484,** 519–523
10. Yount, J. S., Moltedo, B., Yang, Y. Y., Charron, G., Moran, T. M., López, C. B., and Hang, H. C. (2010) Palmitoylome profiling reveals *S*-palmitoylation-dependent antiviral activity of IFITM3. *Nat. Chem. Biol.* **6,** 610–614
11. Huang, I. C., Bailey, C. C., Weyer, J. L., Radoshitzky, S. R., Becker, M. M., Chiang, J. J., Brass, A. L., Ahmed, A. A., Chi, X., Dong, L., Longobardi, L. E., Boltz, D., Kuhn, J. H., Elledge, S. J., Bavari, S., Denison, M. R., Choe, H., and Farzan, M. (2011) Distinct patterns of IFITM-mediated restriction of filoviruses, SARS coronavirus, and influenza A virus. *PLoS Pathog.* **7,** e1001258
12. Weidner, J. M., Jiang, D., Pan, X. B., Chang, J., Block, T. M., and Guo, J. T. (2010) Interferon-induced cell membrane proteins, IFITM3 and tetherin, inhibit vesicular stomatitis virus infection via distinct mechanisms. *J. Virol.* **84,** 12646–12657
13. Lu, J., Pan, Q., Rong, L., He, W., Liu, S. L., and Liang, C. (2011) The IFITM proteins inhibit HIV-1 infection. *J. Virol.* **85,** 2126–2137
14. Feeley, E. M., Sims, J. S., John, S. P., Chin, C. R., Pertel, T., Chen, L. M., Gaiha, G. D., Ryan, B. J., Donis, R. O., Elledge, S. J., and Brass, A. L. (2011) IFITM3 inhibits influenza A virus infection by preventing cytosolic entry. *PLoS Pathog.* **7,** e1002337
15. Kuma, A., Hatano, M., Matsui, M., Yamamoto, A., Nakaya, H., Yoshimori, T., Ohsumi, Y., Tokuhisa, T., and Mizushima, N. (2004) The role of autophagy during the early neonatal starvation period. *Nature* **432,** 1032–1036
16. Gauthier, N. C., Ricci, V., Gounon, P., Doye, A., Tauc, M., Poujeol, P., and Boquet, P. (2004) Glycosylphosphatidylinositol-anchored proteins and actin cytoskeleton modulate chloride transport by channels formed by the *Helicobacter pylori* vacuolating cytotoxin VacA in HeLa cells. *J. Biol. Chem.* **279,** 9481–9489
17. Gauthier, N. C., Monzo, P., Kaddai, V., Doye, A., Ricci, V., and Boquet, P. (2005) *Helicobacter pylori* VacA cytotoxin. A probe for a clathrin-independent and Cdc42-dependent pinocytic pathway routed to late endosomes. *Mol. Biol. Cell* **16,** 4852–4866
18. Yount, J. S., Tsou, L. K., Dossa, P. D., Kullas, A. L., van der Velden, A. W., and Hang, H. C. (2010) Visible fluorescence detection of type III protein secretion from bacterial pathogens. *J. Am. Chem. Soc.* **132,** 8244–8245
19. Kim, W., Bennett, E. J., Huttlin, E. L., Guo, A., Li, J., Possemato, A., Sowa, M. E., Rad, R., Rush, J., Comb, M. J., Harper, J. W., and Gygi, S. P. (2011) Systematic and quantitative assessment of the ubiquitin-modified proteome. *Mol. Cell* **44,** 325–340
20. Wagner, S. A., Beli, P., Weinert, B. T., Nielsen, M. L., Cox, J., Mann, M., and Choudhary, C. (2011) Proteome-wide quantitative survey of *in vivo* ubiquitylation sites reveals widespread regulatory roles. *Mol. Cell. Pro-*

teomics **10,** M111 013284
21. Uittenbogaard, A., Ying, Y., and Smart, E. J. (1998) Characterization of a cytosolic heat-shock protein-caveolin chaperone complex. Involvement in cholesterol trafficking. *J. Biol. Chem.* **273,** 6525–6532
22. Parton, R. G., Hanzal-Bayer, M., and Hancock, J. F. (2006) Biogenesis of caveolae. A structural model for caveolin-induced domain formation. *J. Cell Sci.* **119,** 787–796
23. Mizushima, N., Yoshimori, T., and Levine, B. (2010) Methods in mammalian autophagy research. *Cell* **140,** 313–326
24. Smith, R. A., Young, J., Weis, J. J., and Weis, J. H. (2006) Expression of the mouse fragilis gene products in immune cells and association with receptor signaling complexes. *Genes Immun.* **7,** 113–121
25. Charron, G., Zhang, M. M., Yount, J. S., Wilson, J., Raghavan, A. S., Shamir, E., and Hang, H. C. (2009) Robust fluorescent detection of protein fatty-acylation with chemical reporters. *J. Am. Chem. Soc.* **131,** 4967–4975
26. Wilson, J. P., Raghavan, A. S., Yang, Y. Y., Charron, G., and Hang, H. C. (2011) Proteomic analysis of fatty-acylated proteins in mammalian cells with chemical reporters reveals *S*-acylation of histone H3 variants. *Mol. Cell. Proteomics* **10,** M110 01198
27. Charron, G., Tsou, L. K., Maguire, W., Yount, J. S., and Hang, H. C. (2011) Alkynyl-farnesol reporters for detection of protein *S*-prenylation in cells. *Mol. Biosyst.* **7,** 67–73
28. Ivanov, S. S., Charron, G., Hang, H. C., and Roy, C. R. (2010) Lipidation by the host prenyltransferase machinery facilitates membrane localization of *Legionella pneumophila* effector proteins. *J. Biol. Chem.* **285,** 34686–34698
29. Dietzen, D. J., Hastings, W. R., and Lublin, D. M. (1995) Caveolin is palmitoylated on multiple cysteine residues. Palmitoylation is not necessary for localization of caveolin to caveolae. *J. Biol. Chem.* **270,** 6838–6842
30. Morrow, I. C., Rea, S., Martin, S., Prior, I. A., Prohaska, R., Hancock, J. F., James, D. E., and Parton, R. G. (2002) Flotillin-1/reggie-2 traffics to surface raft domains via a novel golgi-independent pathway. Identification of a novel membrane targeting domain and a role for palmitoylation. *J. Biol. Chem.* **277,** 48834–48841
31. Snyers, L., Umlauf, E., and Prohaska, R. (1999) Cysteine 29 is the major palmitoylation site on stomatin. *FEBS Lett.* **449,** 101–104
32. Huber, T. B., Schermer, B., Müller, R. U., Höhne, M., Bartram, M., Calixto, A., Hagmann, H., Reinhardt, C., Koos, F., Kunzelmann, K., Shirokova, E., Krautwurst, D., Harteneck, C., Simons, M., Pavenstädt, H., Kerjaschki, D., Thiele, C., Walz, G., Chalfie, M., and Benzing, T. (2006) Podocin and MEC-2 bind cholesterol to regulate the activity of associated ion channels. *Proc. Natl. Acad. Sci. U.S.A.* **103,** 17079–17086
33. Voeltz, G. K., and Prinz, W. A. (2007) Sheets, ribbons, and tubules. How organelles get their shape. *Nat. Rev. Mol. Cell Biol.* **8,** 258–264
34. Sällman Almén, M., Bringeland, N., Fredriksson, R., and Schiöth, H. B. (2012) The dispanins. A novel gene family of ancient origin that contains 14 human members. *PLoS One* **7,** e31961
35. Saitou, M., Barton, S. C., and Surani, M. A. (2002) A molecular program for the specification of germ cell fate in mice. *Nature* **418,** 293–300
36. Tanaka, S. S., Yamaguchi, Y. L., Tsoi, B., Lickert, H., and Tam, P. P. (2005) IFITM/Mil/fragilis family proteins IFITM1 and IFITM3 play distinct roles in mouse primordial germ cell homing and repulsion. *Dev. Cell* **9,** 745–756
37. Siegrist, F., Ebeling, M., and Certa, U. (2011) The small interferon-induced transmembrane genes and proteins. *J. Interferon Cytokine Res.* **31,** 183–197
38. Andreu, P., Colnot, S., Godard, C., Laurent-Puig, P., Lamarque, D., Kahn, A., Perret, C., and Romagnolo, B. (2006) Identification of the IFITM family as a new molecular marker in human colorectal tumors. *Cancer Res.* **66,** 1949–1955
39. Seyfried, N. T., Huysentruyt, L. C., Atwood, J. A., 3rd, Xia, Q., Seyfried, T. N., and Orlando, R. (2008) Up-regulation of NG2 proteoglycan and interferon-induced transmembrane proteins 1 and 3 in mouse astrocytoma. A membrane proteomics approach. *Cancer Lett.* **263,** 243–252
40. Zou, K., Hou, L., Sun, K., Xie, W., and Wu, J. (2011) Improved efficiency of female germ line stem cell purification using fragilis-based magnetic bead sorting. *Stem Cells Dev.* **20,** 2197–2204
41. Lange, U. C., Adams, D. J., Lee, C., Barton, S., Schneider, R., Bradley, A., and Surani, M. A. (2008) Normal germ line establishment in mice carrying a deletion of the Ifitm/fragilis gene family cluster. *Mol. Cell. Biol.* **28,** 4688–4696